Validity of Born-Markov master equations for single- and two-qubit systems

Vasilii Vadimov,[1,2,3] Jani Tuorila,[1,2,4] Tuure Orell,[5] Jürgen Stockburger,[6] Tapio Ala-Nissila,[2,7] Joachim Ankerhold,[6] and Mikko Möttönen[1,8]

[1]*QCD Labs, QTF Centre of Excellence, Department of Applied Physics, Aalto University, P.O. Box 13500, FI-00076 Aalto, Espoo, Finland*
[2]*MSP Group, QTF Centre of Excellence, Department of Applied Physics, Aalto University, P.O. Box 11000, FI-00076 Aalto, Espoo, Finland*
[3]*Institute for Physics of Microstructures, Russian Academy of Sciences, 603950 Nizhny Novgorod, GSP-105, Russia*
[4]*IQM, Keilaranta 19, FI-02150 Espoo, Finland*
[5]*Nano and Molecular Materials Research Unit, University of Oulu, P.O. Box 3000, FI-90014, Finland*
[6]*Institute for Complex Quantum Systems and IQST, University of Ulm, 89069 Ulm, Germany*
[7]*Interdisciplinary Centre for Mathematical Modelling, Department of Mathematical Sciences, Loughborough University, Loughborough, Leicestershire LE11 3TU, United Kingdom*
[8]*VTT Technical Research Centre of Finland Ltd., QTF Center of Excellence, P.O. Box 1000, FI-02044 VTT, Finland*

(Received 12 November 2020; revised 27 May 2021; accepted 2 June 2021; published 17 June 2021)

The urgent need for reliable simulation tools to match the extreme accuracy needed to control tailored quantum devices highlights the importance of understanding open quantum systems and their modeling. To this end, we compare here the commonly used Redfield and Lindblad master equations against numerically exact results in the case of one and two resonant qubits transversely coupled at a single point to a Drude-cut ohmic bath. All the relevant parameters are varied over a broad range, which allows us to give detailed predictions about the validity and physically meaningful applicability of the weak-coupling approaches. We characterize the accuracy of the approximate approaches by comparing the maximum difference of their system evolution superoperators with numerically exact results. After optimizing the parameters of the approximate models to minimize the difference, we also explore if and to what extent the weak-coupling equations can be applied at least as phenomenological models. Optimization may lead to an accurate reproduction of experimental data, but yet our results are important to estimate the reliability of the extracted parameter values such as the bath temperature. Our findings set general guidelines for the range of validity of the usual Born-Markov master equations and indicate that they fail to accurately describe the physics in a surprisingly broad range of parameters, in particular, at low temperatures. Since quantum-technological devices operate there, their accurate modeling calls for a careful choice of methods.

DOI: 10.1103/PhysRevB.103.214308

I. GENERAL INTRODUCTION

Precision control and measurement of quantum systems and devices [1,2] have undergone great progress during the recent years. Important applications of this research field in both quantum computing [3–5] and quantum heat engines [6–9] call for in-depth studies of the accuracy of the corresponding theoretical models, especially for open quantum systems, where typically many approximations are utilized to render the problem computationally solvable [10–19]. Most typically, Markovian master equations (MEs) are used, having been historically proven to be simple and effective tools in many scenarios where open quantum systems appear such as in the field of quantum optics [20]. The ME approach can be rigorously justified for the limit of weak coupling and a suitable separation of time scales between the system dynamics and the correlation time of the dissipative reservoir, which, in turn, depends heavily on the reservoir temperature. The most commonly used ME approaches include the Redfield and Lindblad equations [21–23]. The latter is obtained from the former by an additional secular approximation to neglect rapidly oscillating terms in the density operator.

However, such models of open quantum systems require a critical inspection in several important cases of contemporary science and technology. In quantum information, dissipation is typically weak for unitary gate operations, but very high fidelities are pursued, thus setting stringent requirements for the accuracy of the theoretical models [24]. For qubit reset, in contrast [24–30], temporarily strong dissipation is required at least effectively, possibly leading to nontrivial system-reservoir correlations [24,31], and consequently potential initialization errors. In quantum thermodynamics, stronger reservoir coupling combined with finite-time operation typically gives rise to higher performance in terms of total power, and hence the parameter regimes of interest may be very different from those in quantum optics rendering many previous experimental verifications of the models inapplicable [32–34]. Importantly, it is known that some widely adopted models and fundamental physical concepts contradict each other, e.g., the stationary states contradict thermodynamical principles [35–37].

Historically, systematic experimental studies on the validity of the weak-coupling approaches have been challenged by the lack of systematic and predictable tunability of the

relevant parameters such as the coupling strength to a broadband reservoir. Change in the coupling strength may also require adjusting the qubit frequency, which, in turn, may shift the qubit close to a spurious reservoir resonance in an unpredictable manner. Driving certain transitions may effectively provide a tunable dissipation but renders the system intractable for the standard approaches assuming a nondriven system. Redesign and fabrication of a new sample may readily produce parameters in the desired range, but this is a very slow and resource-intensive approach.

The recent development of a quantum-circuit refrigerator (QCR) [38–40] has introduced the solid-state-qubit community to a simple device that provides orders-of-magnitude tunability in the system-reservoir coupling strength with minimal effect on the system parameters. Thanks to this tunability, the QCR has thus far been used to observe the Lamb shift arising from a broadband reservoir of an engineered quantum system [41] and has the potential to enhance, for example, qubit initialization [42], quantum-thermodynamic devices [43], quantum-state-engineering protocols [44–47], and synthetic quantum matter [48–50]. Together with the generally expanding experimental toolbox for quantum technology, QCR motivates us to benchmark the validity and accuracy of widely used approximate methods for open quantum systems against numerically exact solutions. Our theoretical study may thus work as a road map for various future experiments in the pursuit of computationally feasible and accurate models.

In parallel to these developments, advanced descriptions of reduced open quantum dynamics have been formulated and applied to a variety of systems. These approaches are based on a nonperturbative representation of the reduced density matrix in terms of path integrals pioneered by Feynman and Vernon [10,51]. Accordingly, path-integral Monte Carlo techniques have been shown to provide insight into subtle qubit-reservoir correlations in regimes not accessible by other means [52]. Often more efficient and with a broader range of applicability are stochastic representations of the path-integral dynamics [53,54], in particular, the stochastic Liouville–von Neumann equation (SLN) [33,55–57] and its version for ohmic dissipation [stochastic Liouville equation with dissipation (SLED)] [58,59].

This paper is organized as follows: After this general introduction to the field of research, we proceed in Sec. II to discuss in an introductory manner the different master equations used in our study, and we especially elaborate on the Born-Markov approximation. In Sec. III, we introduce the microscopic Hamiltonian and define the error functional we use to study the difference between the evolution operators given by the different approaches. Sections IV and V provide our most important numerical results on the single- and two-qubit cases, respectively. Appendixes A and B provide mathematical details of the master equations used and the numerically exact stochastic method.

II. INTRODUCTION TO THE MODELS USED

The formal requirements needed to achieve consistency between the Lindblad approach and the corresponding full microscopic model have been thoroughly studied [12,60]. Importantly, the dissipator terms in both Redfield and Lindblad equations do not directly correspond to any Hamiltonian operator of the microscopic model. They are rather a compact and approximate representation of the processes which amount to lowest-order emission and absorption of energy quanta.

The Born-Markov (BM) approximation is at the heart of the Redfield equation. Here, one applies the lowest-order nontrivial perturbation theory for the system-reservoir coupling, where the effect of the system-reservoir correlations on the evolution are neglected. In addition, one effectively applies coarse graining over time scales much longer than the characteristic time scale of the system Hamiltonian and assumes that the correlation time of the reservoir is much shorter than the resulting decay time. In addition to the above BM approximation, an additional assumption of a separable coupling forms the basis of the standard Redfield master equation.

For a broadband reservoir, the correlation time is of the order of the thermal time $\hbar\beta = \hbar/(k_{\mathrm{B}}T)$, where $\hbar$ is the reduced Planck constant, k_{B} is the Boltzmann constant, and T is the reservoir temperature. Thus the BM approximation does not necessarily imply a white-noise limit. In fact, the separation of time scales characterizing the BM approximation is typically considered between the reservoir correlation time and the time scales of relaxation and dephasing processes caused by the system-reservoir interaction.

The reduced dynamics induced by the Redfield equation lacks a fundamental property of quantum channels: It is not completely positive. Even negative eigenvalues of the reduced density operator itself may appear. Neglecting quickly oscillating components of the density operator, a method generally referred to as the secular approximation, remedies this shortcoming and leads to the Lindblad equation. However, this advantage comes at the price of an additional condition of validity, namely, the level spacings of the system must greatly exceed the decay rates. This is typically a stricter requirement than the weak-coupling assumption in the BM approximation, and consequently, the Redfield equation may in many cases provide a more accurate model although not guaranteeing complete positivity. We note that recently this shortcoming has been remedied by the derivation of a Lindblad-like master equation based on expansion in terms of the correlation between the bath and the system instead of the coupling strength [61].

The secular approximation discussed above also includes a subtlety sometimes overlooked in the literature. Namely, the basis in which the secular approximation is carried out defines also the basis in which the dissipative transitions take place. This effect is pronounced in driven or multipartite systems, where one may, for example, choose a local approach, where the basis is chosen as the instantaneous eigenbasis of the individual constituents of the multipartite system, or the global approach, where one uses the eigenbasis of the full multipartite Hamiltonian taking into account its possible temporal trajectory [35–37,62–66]. A temporally local approach in the case of external driving has been observed to lead to unphysical results, for example, in Cooper pair pumping [67–70], and constitutes an interesting research direction. In this paper, however, we focus on nondriven systems and benchmark the validity of the local and global Lindblad equations and the Redfield equation against numerically exact qubit dynamics.

Exact methods beyond the BM family of open-quantum-system approaches are well established [10,51,54,58,59,71] but more complicated and computationally expensive. Beyond the Born approximation, reservoirs which are Gaussian can still be fully characterized by a two-time correlator. A somewhat loose but intuitively appealing characterization of this generalization can be given as follows: Gaussianity beyond the Born approximation implies that the high-order emission and absorption terms become relevant but are reducible in the spirit of Wick's theorem. This scenario enables an exact description of the corresponding quantum dynamics through path integrals in the form of the Feynman-Vernon influence functional [10,51,71]. The influence functional is a nonlocal functional of the paths describing the propagation of the reduced density operator, and hence challenging to solve numerically. This inconvenience can be circumvented by a stochastic unraveling of the influence functional [54] in a similar fashion to the Hubbard-Stratonovich transform. Thus one obtains a time-local master equation for the reduced system density operator which is of a computational complexity equal to that of the weak-coupling equations except that it is subject to two noise terms in the general case, or a single noise term in the case of ohmic dissipation [58,59]. We use the latter approach, referred to as stochastic Liouville equation with dissipation (SLED), as a benchmark to check the validity of the above-discussed BM approaches. The SLED has been proven to combine high numerical efficiency with high accuracy in broad ranges of parameter space together with the versatility to be adapted easily to various systems; see, e.g., Refs. [33,56]. The existence of the noise terms necessitates that one ensemble-average the density operators obtained for individual noise realizations to obtain the system density operator, which renders this method computationally much heavier than the weak-coupling approaches. Nevertheless, parallel computing can be utilized to obtain exact dynamics of low-dimensional open quantum systems.

The above methods based on stochastic equations are not the only numerically exact methods of simulation of dynamics of the open quantum systems. There are frequently used techniques such as hierarchical equations of motion (HEOMs) [72,73], the quasiadiabatic propagator path integral (QUAPI) [74,75], and the time-evolving density matrix using orthogonal polynomials algorithm (TEDOPA) [76,77]. All exact methods provide identical answers within the numerical accuracy, which justifies our choice of SLED in the parameter regime considered in this paper. In this paper we use SLED because it was previously benchmarked [24] and we find it well suitable for the considered system and range of parameters.

III. MICROSCOPIC HAMILTONIAN AND ERROR OF PERTURBATIVE PROPAGATION

In this paper, we study single- and two-qubit systems embedded in a large number of reservoir degrees of freedom, a situation that generically appears in solid-state implementations. A typical realization of this scenario consists of electromagnetic modes interacting with a superconducting or a semiconductor qubit system, thus causing decoherence in the latter. If the quantum fluctuations caused by these reservoir modes are Gaussian in nature, they can be modeled by a set of harmonic oscillators bilinearly coupled to the qubit system. Accordingly, we assume a general Hamiltonian of the form

$$\hat{H} = \hat{H}_{\mathrm{S}} + \sum_k \hbar\Omega_k \hat{b}_k^\dagger \hat{b}_k + \hat{q}\hat{\xi}, \tag{1}$$

where $\hat{H}_{\mathrm{S}}$ is the Hamiltonian of a single- or two-qubit system, $\hat{q}$ is the system part of the system-reservoir coupling operator, and the corresponding reservoir operator is given by

$$\hat{\xi} = \sum_k g_k(\hat{b}_k^\dagger + \hat{b}_k). \tag{2}$$

For this type of model, the effective impact of the reservoir on the qubit system is characterized by the reservoir temperature $1/\beta$ and the weighted spectral density $J(\omega) = \pi \sum_k g_k^2 \delta(\omega - \Omega_k)/\hbar$. Below, we assume an Ohmic-type distribution with a high cutoff frequency ω_{c} such that we obtain in the continuum limit

$$J(\omega) = \frac{\eta\omega}{\left(1+\omega^2/\omega_{\mathrm{c}}^2\right)^2}. \tag{3}$$

The usual Drude cutoff term appears in squared form here to avoid divergences of the total noise power of the reservoir. Ohmic-type reservoirs can be found in a broad class of qubit systems, particularly in superconducting devices. In experiments, they may accurately capture qubit-reservoir interactions only in the moderate- to high-frequency range, whereas at very low frequencies non-Ohmic behavior is typical and system dependent, for example, in the form of $1/f$ noise. Assuming a well-calibrated system, however, the latter are of minor relevance on the time scales of qubit control and error correction and are thus not studied in this paper. Here, we rather present a detailed analysis of perturbative weak-coupling treatments in describing with sufficient accuracy the dissipative qubit dynamics in comparison with exact results.

In order to quantify the difference in the numerical performance between the perturbative and the exact methods, we introduce the superoperator $\mathcal{T}(t)$, which transforms an initial reduced system density matrix $\rho_{\mathrm{S}}(0)$ to that at time t as

$$\hat{\rho}_{\mathrm{S}}(t) = \mathcal{T}(t)\hat{\rho}_{\mathrm{S}}(0). \tag{4}$$

We estimate the accuracy of the BM approaches by calculating the distance

$$\Delta(t) = ||\overline{\mathcal{T}}_{\mathrm{BM}}(t) - \overline{\mathcal{T}}_{\mathrm{SLED}}(t)||/2 \tag{5}$$

between normalized evolution superoperators of the BM type and of the corresponding numerically exact solution obtained with the SLED. The normalization of a superoperator $\mathcal{A}$ is defined as $\overline{\mathcal{A}} = \mathcal{A}/||\mathcal{A}||$, where the Frobenius norm $||\cdot||$ is given by

$$||\mathcal{A}|| = \sqrt{\sum_{i=1}^{N^2}\sum_{j=1}^{N^2} |\mathcal{A}_{ij}|^2}, \tag{6}$$

with $\mathcal{A}_{ij}$ being the matrix elements of $\mathcal{A}$ in the chosen basis and N denoting the dimension of the system Hilbert space, i.e., $N = 2$ for the single-qubit system and $N = 4$ for the two-qubit system.

In the case of time-independent Hamiltonians, the evolution superoperator corresponding to a BM master equation can be formally represented as

$$\mathcal{T}(t) = e^{\mathcal{L}t}, \tag{7}$$

where $\mathcal{L}$ is the Liouvillian superoperator of the open quantum system defined by $\dot{\rho}_{\rm S}(t) = \mathcal{L}\rho_{\rm S}(t)$ and including the nonunitary dissipative terms of the master equation. The nonunitary evolution superoperator $\mathcal{T}_{\rm SLED}(t)$ [see Eq. (4)] for the numerically exact SLED solution is constructed by solving the SLED using N^2 linearly independent initial conditions for the density operator $\hat{\rho}_{\rm S}(0)$.

Furthermore, a temporally independent figure to quantify the accuracy of a BM evolution is obtained by the maximum distance from the SLED defined as

$$\Delta_{\rm max} = \max_{t\in[0,\infty)} \Delta(t), \tag{8}$$

Since we are considering a nondriven decaying system, the maximum is attained in practice at a finite time.

In a physical setup, the parameters which enter the above models are typically not known *a priori*, but are adjusted after obtaining information from the system. Hence we also carry out a study where we minimize $\Delta_{\rm max}$ by optimizing the parameters of the system and the bath and those determining their interaction. This optimization procedure may be interpreted as a simulation of a typical experimental situation in which the measurement data correspond to those of the SLED and the system parameters and dissipation rates are extracted to fit a BM model for the open quantum system (assuming structurally the same system and a system-reservoir coupling Hamiltonian). However, our detailed analysis demonstrates below that such a procedure may not always provide accurate predictions of the parameter values, especially in the case of moderate or strong system-reservoir coupling or if the interaction parameters with the reservoir are tuned during the evolution. One should be even more cautions about making extrapolations of experimental data deep into unmapped parameter regimes based on the fits.

IV. SINGLE-QUBIT RESULTS

We start with the single-qubit case, where the system (Fig. 1(a))

$$\hat{H}_{\rm S} = \hbar\omega_{\rm q}\hat{\sigma}^+\hat{\sigma}^- \tag{9}$$

is coupled to the bath through the operator $\hat{q} = \hat{\sigma}^+ + \hat{\sigma}^- = \hat{\sigma}^x$ with the parameter $\kappa = 2\hbar\eta\omega_{\rm q}$ controlling the coupling strength to the bath. Here, $\hat{\sigma}^+ = (\hat{\sigma}^-)^\dagger = |{\rm e}\rangle\langle{\rm g}|$, where $|{\rm g}\rangle$ and $|{\rm e}\rangle$ are the ground and the excited state of the qubit, respectively.

In Fig. 2 we show the distance $\Delta_{\rm max}$ for the BM solutions (Redfield and Lindblad) calculated for dimensionless parameters $\kappa/\omega_{\rm q}$ and $\omega_{\rm q}\hbar\beta$. As expected their performance deteriorates with increasing qubit-reservoir coupling, where the Redfield solution covers a broader domain with acceptable accuracy.

What is not expected at first glance is that the accuracy of BM approaches deteriorates with the decrease in the bath temperature while staying in the weak-coupling regime $\kappa \ll$

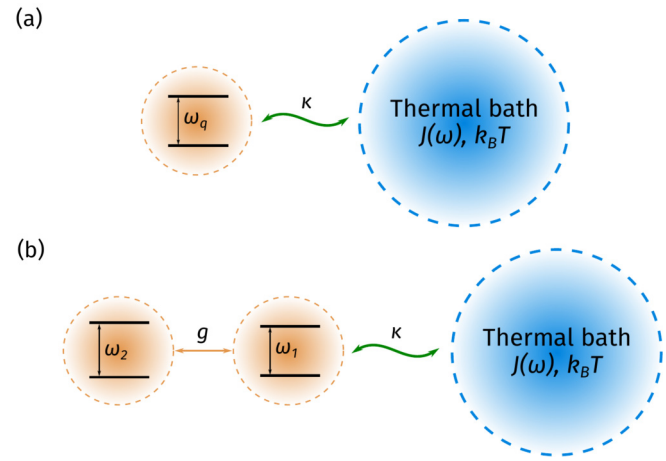

FIG. 1. (a) Single- and (b) two-qubit system coupled to the thermal bath, or reservoir, with the spectral density $J(\omega)$ and temperature T. The parameter κ characterizes the coupling strength between the qubits and the reservoir, saturating to the decay rate in the zero-coupling limit. The angular frequencies of the qubits are denoted by $\{\omega_k\}_{k=\rm q,1,2}$. In the case of the two-qubit system, the qubits are coupled to each other with the coupling strength determined by a parameter g.

$\omega_{\rm q}$. A possible reason for this could be disregarding the Lamb shift, which should be significant in the low-temperature case. In order to verify this, we perform BM calculations including the Lamb-shifted qubit frequency $\Omega_{\rm q}$ given by the following expression [10,24]:

$$\Omega_{\rm q} = \omega_{\rm eff}\left\{1 + 2K\left[{\rm Re}\,\psi\left(i\frac{\hbar\beta\omega_{\rm eff}}{2\pi}\right) - \ln\left(\frac{\hbar\beta\omega_{\rm eff}}{2\pi}\right)\right]\right\}^{1/2}, \tag{10}$$

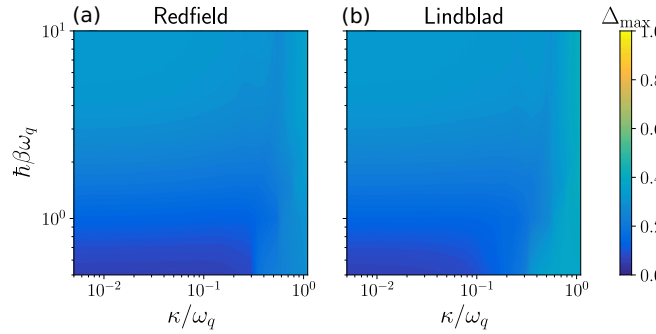

FIG. 2. (a) and (b) Maximum value of the distance $\Delta_{\rm max}$ obtained with nonoptimized values of κ, β, and the qubit angular frequency $\omega_{\rm q}$. The nonunitary temporal-evolution superoperator $\mathcal{T}_{\rm SLED}(t)$ [see Eq. (4)] is constructed numerically by solving the SLED using initial states $\hat{\rho}^x_{\rm SLED}(0) = |\sigma_x, +\rangle\langle\sigma_x, +|$, $\hat{\rho}^y_{\rm SLED}(0) = |\sigma_y, +\rangle\langle\sigma_y, +|$, $\hat{\rho}^z_{\rm SLED}(0) = |\sigma_z, +\rangle\langle\sigma_z, +|$, and $\hat{\rho}^I_{\rm SLED}(0) = \frac{1}{2}\hat{I}$, where $|\sigma_i, +\rangle$ is the excited eigenstate of the $\hat{\sigma}_i$ operator with $i = x, y, z$ and $\hat{I}$ is the identity operator. The number of samples in the SLED solutions is $N_{\rm traj} = 10^5$, and we have used the cutoff frequency $\omega_{\rm c}/\omega_{\rm q} = 50$. For each pair $\{\kappa, \beta\}$, the trace distance is calculated for times $[0, 10\kappa_T^{-1}]$, where $\kappa_T = \kappa\coth(\hbar\beta\omega_{\rm q}/2)$.

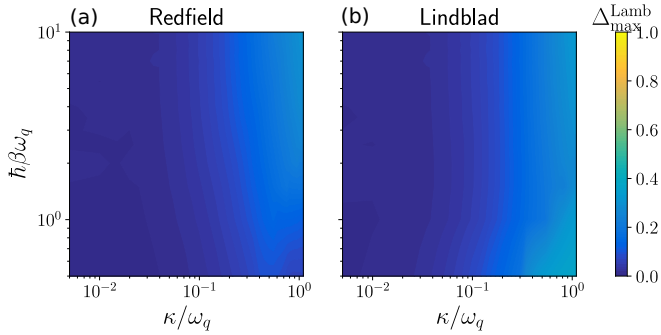

FIG. 3. (a) and (b) Maximum value of the distance $\Delta_{\max}$ obtained with nonoptimized values of κ, β, and the Lamb-shift-corrected qubit angular frequency Ω_{q} [see Eq. (10)].

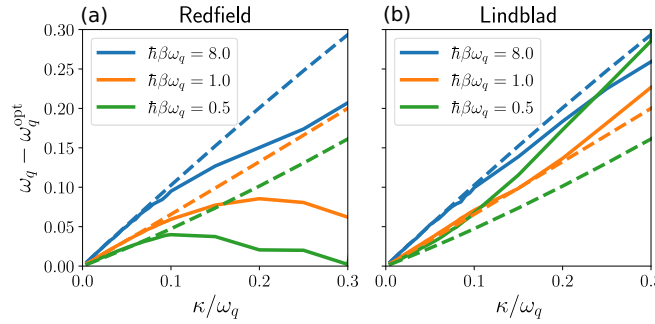

FIG. 4. (a) and (b) Correction to the qubit frequency obtained by the optimization procedure $\omega_{\mathrm{q}} - \omega_{\mathrm{q}}^{\mathrm{opt}}$ (solid lines) and the analytically predicted Lamb shift $\omega_{\mathrm{q}} - \Omega_{\mathrm{q}}$ (dashed lines).

where $\psi(x)$ is the digamma function, $\omega_{\mathrm{eff}} = G(\omega_{\mathrm{q}}/\omega_{\mathrm{c}})^{K/(1-K)}\omega_{\mathrm{q}}$, $K = \kappa/(2\pi\omega_{\mathrm{q}})$, $G = [\Gamma(1-2K)\cos(\pi K)]^{1/[2(1-K)]}$, and $\Gamma(x)$ is the gamma function. Note that for simplicity, we do not differentiate here between the Lamb and Stark shifts, but refer to the total environment-induced frequency shift of the system as the Lamb shift.

Figure 3 shows the distance between the SLED and BM solutions with the Lamb-shifted qubit frequency taken into account. The performance of the weak-coupling approaches is significantly improved, and the regime of their applicability is extended to lower temperatures.

We also provide an optimized BM solution by finding for a given set of parameters those values for $\{\kappa^{\mathrm{opt}}, \beta^{\mathrm{opt}}, \omega_{\mathrm{q}}^{\mathrm{opt}}\}$ that minimize the maximal value of the distance $\Delta_{\max}$, i.e., $\Delta_{\max}^{\mathrm{opt}} = \Delta_{\max}(\kappa^{\mathrm{opt}}, \beta^{\mathrm{opt}}, \omega^{\mathrm{opt}})$. Technically, the optimization is carried out using the Powell minimization method available as one of the standard methods in the SCIPY numeric library [78].

It is an interesting question whether the optimization procedure can capture the Lamb shift originating from the interaction with the environment. In order to answer this, we compare the correction to the qubit frequency obtained by the optimization procedure $\omega_{\mathrm{q}} - \omega_{\mathrm{q}}^{\mathrm{opt}}$ with the analytically predicted Lamb shift $\omega_{\mathrm{q}} - \Omega_{\mathrm{q}}$. This comparison is shown in Fig. 4. Apparently, the corrections are consistent with each other only in the weak-coupling regime $\kappa/\omega_{\mathrm{q}} \lesssim 0.1$.

Figure 5 displays areas of acceptable accuracy of nonoptimized and optimized BM methods, where we consider a maximal distance of $\Delta_{\max} = 0.1$ as a threshold. While we confirm that the nonoptimized BM solutions without the Lamb-shift correction are limited by sufficiently elevated temperatures $\hbar\beta\omega_{\mathrm{q}} \lesssim 1$ and low coupling strengths between the bath and the qubit $\kappa/\omega_{\mathrm{q}} \ll 1$, we find that the optimized BM solutions as well as BM solutions with the Lamb shift taken into account approximate the SLED solution quite well even at lower temperatures up to $\hbar\beta\omega_{\mathrm{q}} \approx 10$. This implies that the dynamics of the qubit can be effectively, i.e., by properly tuned parameters, captured by Markovian dynamics in the weak-coupling limit. However, in a broad range the values of these optimized parameters differ substantially from the bare ones (see Figs. S1– S3 of the Supplemental Material [79]) and even physically cannot always be considered as meaningful. In fact, they are outside the range of formal validity of the underlying approximations of the BM approaches and/or are not reasonable given typical experimental setups. More specifically, the optimization parameters should be trusted only in the weak-coupling regime $\kappa \lesssim 0.3\omega_{\mathrm{q}}$.

V. TWO-QUBIT RESULTS

Let us consider here two linearly coupled qubits described by the system Hamiltonian (Fig. 1(b))

$$\hat{H}_{\mathrm{S}} = \hbar\omega_1\hat{\sigma}_1^+\hat{\sigma}_1^- + \hbar\omega_2\hat{\sigma}_2^+\hat{\sigma}_2^- + \frac{\hbar g}{2}\hat{\sigma}_1^x\hat{\sigma}_2^x, \tag{11}$$

where the angular frequency of qubit k is denoted by ω_k and the qubit-qubit coupling strength is denoted by g. In the total Hamiltonian, only the first qubit denoted by the subscript 1 is coupled to the bath through the operator $\hat{q} = \hat{\sigma}_1^x$. We consider two types of weak-coupling treatments: For weak qubit-qubit coupling, one typically uses the local Lindblad (LL) master equation, where the dissipators induce transitions between the eigenstates of the bare qubit 1. In contrast, the global Lindblad (GL) master equation describes transitions in the two-qubit eigenbasis.

For LL, the master equation of the reduced density operator of the two-qubit system is expressed as

$$\frac{d\hat{\rho}_{\mathrm{S}}}{dt} = -\frac{i}{\hbar}[\hat{H}_{\mathrm{S}}, \hat{\rho}_{\mathrm{S}}] + \frac{\kappa}{2}[N(\omega_1)+1][2\hat{\sigma}_1^-\hat{\rho}_{\mathrm{S}}\hat{\sigma}_1^+ - \{\hat{\sigma}_1^+\hat{\sigma}_1^-, \hat{\rho}_{\mathrm{S}}\}] + \frac{\kappa}{2}N(\omega_1)[2\hat{\sigma}_1^+\hat{\rho}_{\mathrm{S}}\hat{\sigma}_1^- - \{\hat{\sigma}_1^-\hat{\sigma}_1^+, \hat{\rho}_{\mathrm{S}}\}], \tag{12}$$

where $N(\omega) = 1/[\exp(\hbar\beta\omega) - 1]$ is the bosonic occupation.

Further analytical progress is possible if one applies the rotating-wave approximation, i.e., if one replaces the qubit-qubit coupling term $\sigma_1^x\sigma_2^x$ in the Hamiltonian by $\hbar(\hat{\sigma}_1^+\hat{\sigma}_2^- + \hat{\sigma}_1^-\hat{\sigma}_2^+)g/2$. Consequently, we arrive at the following equation of motion, which is expressed, for simplicity, in the zero-temperature limit:

$$\frac{d^2\langle\hat{\sigma}_2^-\rangle}{dt^2} + \left(i\delta_{12} + \frac{\kappa}{2}\right)\frac{d\langle\hat{\sigma}_2^-\rangle}{dt} + \frac{g^2}{4}\langle\hat{\sigma}_2^-\rangle = 0, \tag{13}$$

where $\delta_{1,2} = \omega_1 - \omega_2$ is the detuning between the qubits. Thus the exponential relaxation of the system is characterized by two complex-valued decay rates λ_1 and λ_2, which, in the

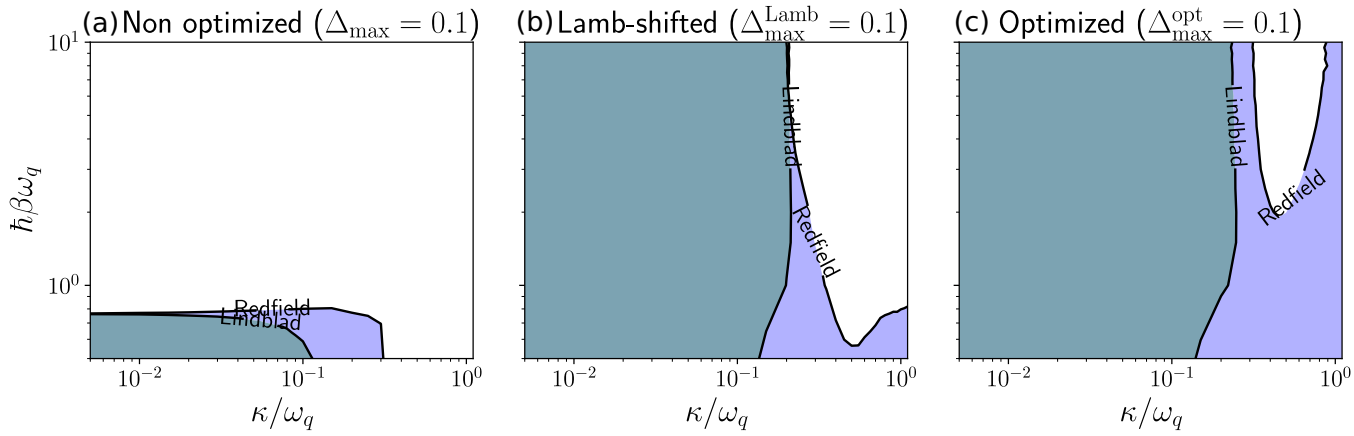

FIG. 5. Diagrams showing the maximal error contour lines $\Delta_{\max} = 0.1$ in the case of a single qubit coupled to the environment. From left to right, we have the nonoptimized (a), Lamb-shift-corrected (b), and optimized (c) Lindblad (green) and Redfield (blue) data.

case of resonant qubits $\delta_{1,2} = 0$, turn out to be

$$\lambda_{1,2} = \frac{\kappa}{4} \pm \frac{1}{2}\sqrt{\frac{\kappa^2}{4} - g^2}. \tag{14}$$

Accordingly, in the case of weak damping, $\kappa \ll g$, qubit 2 displays underdamped oscillations towards its bare ground state with the amplitude relaxation rate $\kappa/4$. In the opposite limit, $\kappa \gg g$, a separation of time scales occurs, where one of the resulting rates, $\kappa/2$, by far exceeds the other, $g^2/(2\kappa)$. The latter rate determines the full equilibration time scale of the system. From a simulation point of view, this phenomenon implies that the computation of the asymptotic long-time behavior requires significant computational resources. Hence, instead of simulating the full-length equilibration dynamics of the system, we monitor the quantum evolution only for a fixed time interval $[0, T]$, where we use $T = 2 \times 10^3/\omega_1$, and subsequently analyze whether the system converged into its steady state or not. To this end, we compute the least negative eigenvalue $\lambda_{\min}$ of the Liouvillian and compare T with the relaxation time estimated by $-3/\mathrm{Re}(\lambda_{\min})$. If T exceeds the relaxation time, we conclude that the system has reached equilibrium.

According to this procedure, we study the accuracy of the LL equation, the GL equation, and the Redfield equation (see Appendix A for details on the weak-coupling equations). For the sake of clarity, we focus on resonant qubits $\omega_1 = \omega_2$ throughout this section. In the opposite case, $|\omega_1 - \omega_2| \gg g$, the coupling between the qubits appears as a weak perturbation to the local eigenstates, and it is expected that the effect of the reservoir, which directly interacts with the first qubit, may be described using the weak-coupling approaches for the second qubit even in the regime $\kappa \gtrsim g$, provided that $\kappa \ll \omega_1, \omega_2$.

For which parameters does one expect that the weak-coupling approaches provide reliable predictions? In order to justify the secular approximation, the coupling strength to the reservoir characterized by κ should be very weak compared with the smallest distance between the energy levels of the Hamiltonian (11), which is equal to g for the qubits in resonance. Thus for our case of resonant qubits, we expect the GL equation to be valid only for $\kappa \ll g$. The Redfield equation partially cures this deficiency since it relies only on the BM approximations but does not invoke the secular approximation. Strictly speaking, all three approaches call for $\hbar\kappa\beta \ll 1$ to justify the Markov approximation (see Appendix A for details).

Figure 6 shows the maximum distance between the SLED solution and each weak-coupling approach, $\Delta_{\max}$, as a function of the qubit-bath and qubit-qubit coupling strengths, κ and g, respectively, for high ($\hbar\omega_1\beta = 0.1$) and intermediate ($\hbar\omega_1\beta = 1$) temperatures. We observe that in the high-temperature regime the Redfield equation reproduces the exact dynamics for the whole considered range of parameters, whereas the Lindblad approaches based on secular approximations have significant limitations. As expected, the GL approach is valid only in the region $g \gg \kappa$, while the LL is the most accurate for $\kappa/\omega_1, g/\omega_1 \ll 1$. The poor performance of the GL equation is due to the neglected slowly oscillating terms with the frequency of order g owing to the secular approximation. These terms appear due to the splitting of the resonant qubit levels, which implies that the resonant situation is the most problematic one, whereas for nonresonant qubit systems with all the levels sufficiently separated, the accuracy of the GL equation is expected to be higher. Interestingly, the situation is different at intermediate temperatures $\hbar\beta\omega_1 = 1$ even for the Redfield treatment as shown in Fig. 6(d). The solutions given by the SLED and the BM approaches are noticeably different, which is largely explained by the lack of a Lamb shift for the weak qubit-bath coupling and by the violation of the BM conditions for strong coupling.

We anticipate that the above-observed discrepancies between the Born-Markov approaches and the SLED solution at low temperatures are caused by the disregard of the Lamb shift which is induced in the system by the dissipative environment. To study the Lamb shift, we take into account the corresponding coherent correction to the system Hamiltonian. For the Redfield equation, this correction is given by Eq. (A20), and in general, it does not commute with the bare system Hamiltonian. For consistency with the secular approximation to the Redfield equation, however, we take into account only the diagonal terms of this correction in the GL equation, resulting in Eq. (A21). For the LL approach we calculate the

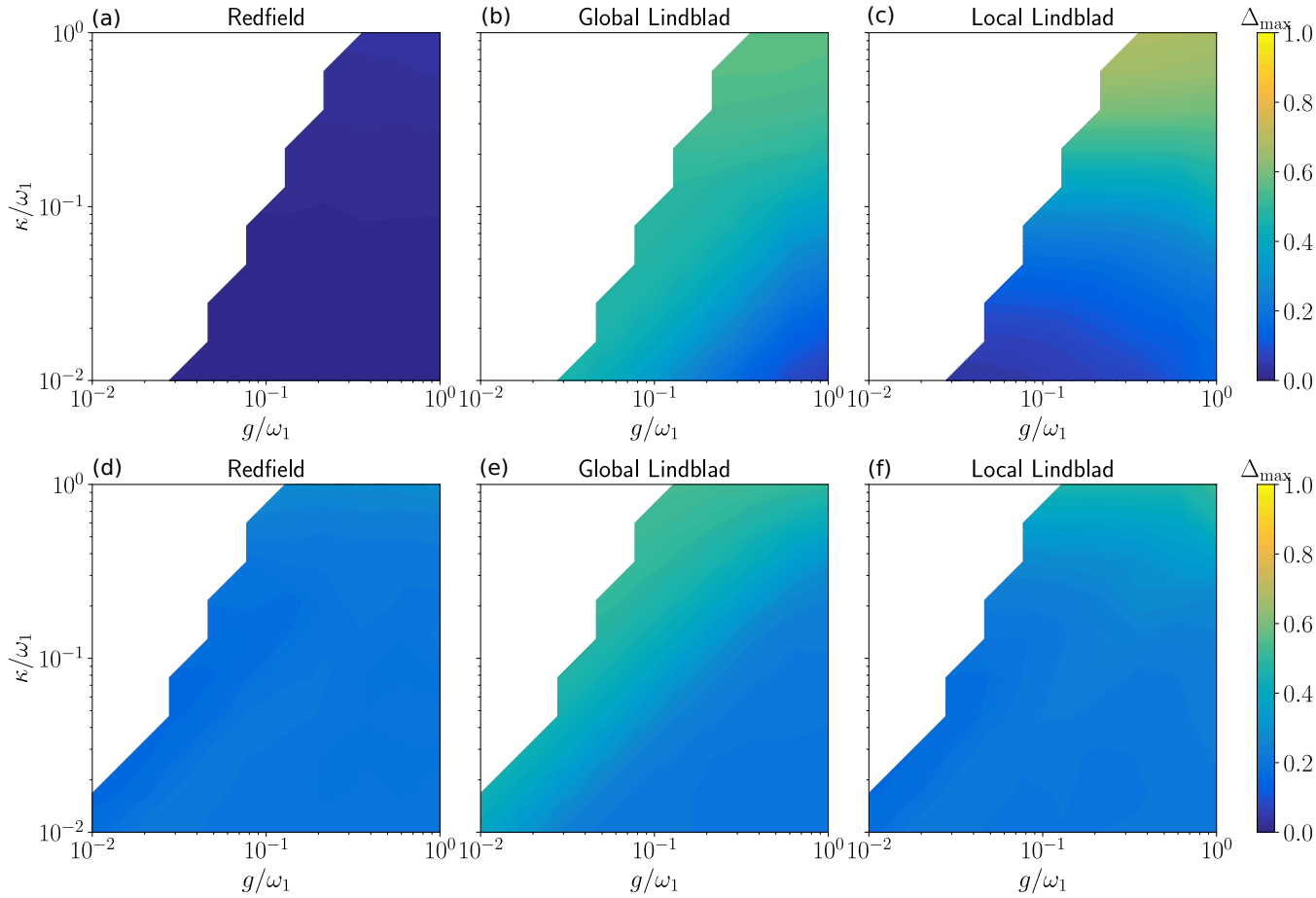

FIG. 6. Distance $\Delta_{\max}$ for nonoptimized values of parameters at the (a)–(c) high temperature $\hbar\omega_1\beta = 0.1$ and (d)–(f) intermediate temperature $\hbar\omega_1\beta = 1$. The number of samples in the SLED solutions is $N_{\text{traj}} = 10^4$, and we have used the cutoff frequency $\omega_c/\omega_1 = 50$. For each pair $\{g, \kappa\}$, the distance is calculated for times $[0, 2 \times 10^3\omega_1^{-1}]$. The white color corresponds to the range of parameters for which the steady state has not been achieved.

Lamb shift using (A21) such that the system Hamiltonian and its eigenstates correspond to those of uncoupled qubits. Due to this approximation only the first qubit, which is coupled to the dissipative environment, acquires the Lamb shift. In the high-temperature regime $\hbar\beta\omega_1 = 0.1$, taking account of the Lamb shift does not lead to any significant differences in the maximum distance between the SLED solution and the BM approaches. Here, $\Delta_{\max}$ almost coincides with Fig. 6(a). However, for the intermediate temperature, taking account of the Lamb shift significantly improves the accuracy of all BM approaches as revealed by comparing the Lamb-shift-corrected data in Fig. 7 with that without the Lamb shift in Fig. 6.

Next, we optimize the parameters of the two-qubit system and the bath used in the BM equations in order to minimize the distance $\Delta_{\max}$ with respect to the SLED solution. Here, the Lamb shift has a generic form of a 4×4 Hermitian correction to the Hamiltonian. Since an implementation of a reliable optimization with respect to the corresponding ten parameters together with an involved interpretation of the results appears challenging, we optimize only with respect to the bath parameters β and κ. The optimized distance $\Delta_{\max}^{\text{opt}}$ as a function of the coupling parameters g and κ is shown in Fig. 8 for high and intermediate temperatures. For the high temperature, the optimization seems to noticeably improve the accuracy of the BM approaches only in the strong-coupling regime, where, unfortunately, the BM approaches are inapplicable. For the intermediate temperature, significant improvement is visible also for weak coupling.

Figure 9 provides $\Delta_{\max}$ at a low temperature of $\hbar\beta\omega_1 = 5$. Owing to the large number of samples needed at this temperature to reach numerical convergence for SLED, we fix $g = 0.1 \times \omega_1$. With these parameters, the nonoptimized purely dissipative weak-coupling approaches fail to describe the dynamics of the system even for $\kappa \ll g \ll \omega_1$, whereas the Lamb-shifted and the optimized solutions display much better performance, at least in certain parameter ranges, thanks to properly accounting for the Lamb shift caused by the environment.

Although the optimized weak-coupling model may relatively accurately yield the exact dynamics, it may still be, depending on the parameters, that it misses important physics which may render the extracted parameter values questionable. Fortunately, this is not the case in our study except for the highest considered qubit-bath coupling strengths as we further discuss in the Supplemental Material [79].

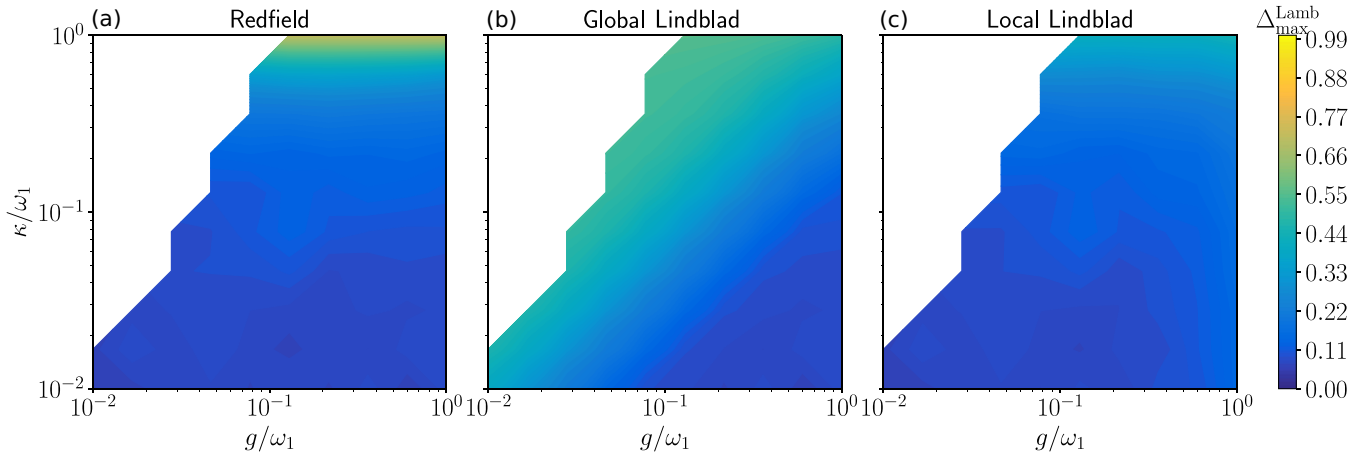

FIG. 7. Distance $\Delta_{\max}^{\mathrm{opt}}$ for optimized values of parameters at the (a)–(c) high temperature $\hbar\omega_1\beta = 0.1$ and (d)–(f) intermediate temperature $\hbar\omega_1\beta = 1$. The white color corresponds to the range of parameters for which the steady state has not been achieved.

VI. SUMMARY AND CONCLUSIONS

Let us summarize our main results. For a single qubit with angular frequency ω_{q} and realistic microscopically derived model parameters, we find that the approximate approaches are valid ($\Delta_{\max} < 0.1$) only at high bath temperatures, $T \gtrsim 1.5 \times \hbar\omega_{\mathrm{q}}/k_{\mathrm{B}}$ ($\omega_{\mathrm{q}}\hbar\beta \lesssim 0.7$), and for low relaxation rates, $\kappa < 0.1 \times \omega_{\mathrm{q}}$, for the Lindblad approaches and slightly greater values $\kappa < 0.3 \times \omega_{\mathrm{q}}$ for the Redfield approach. The optimization of the system parameters allows us to expand the validity of these approaches to lower temperatures, at

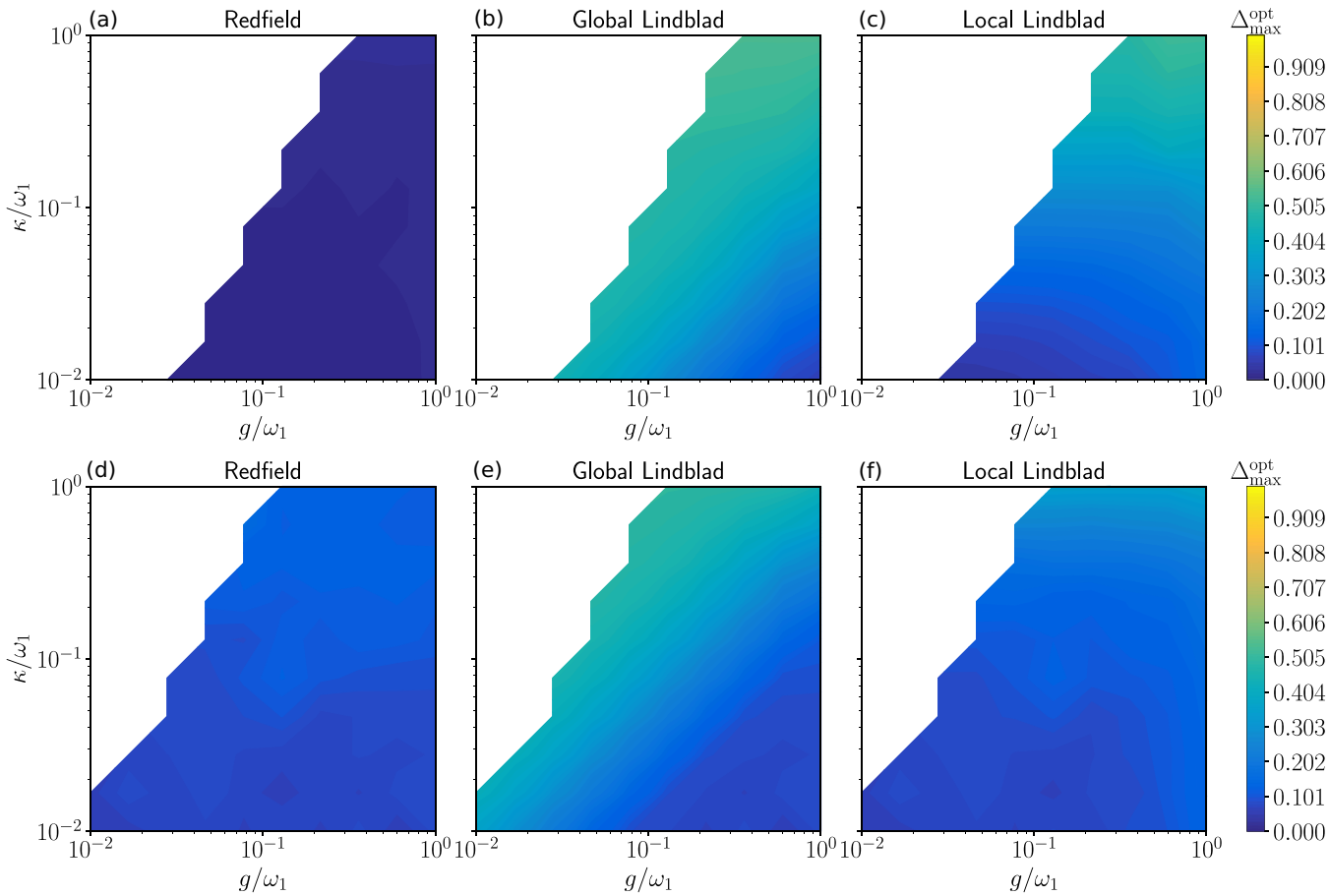

FIG. 8. Distance $\Delta_{\max}^{\mathrm{opt}}$ for optimized values of parameters at the (a)–(c) high temperature $\hbar\omega_1\beta = 0.1$ and (d)–(f) intermediate temperature $\hbar\omega_1\beta = 1$. The white color corresponds to the range of parameters for which the steady state has not been achieved.

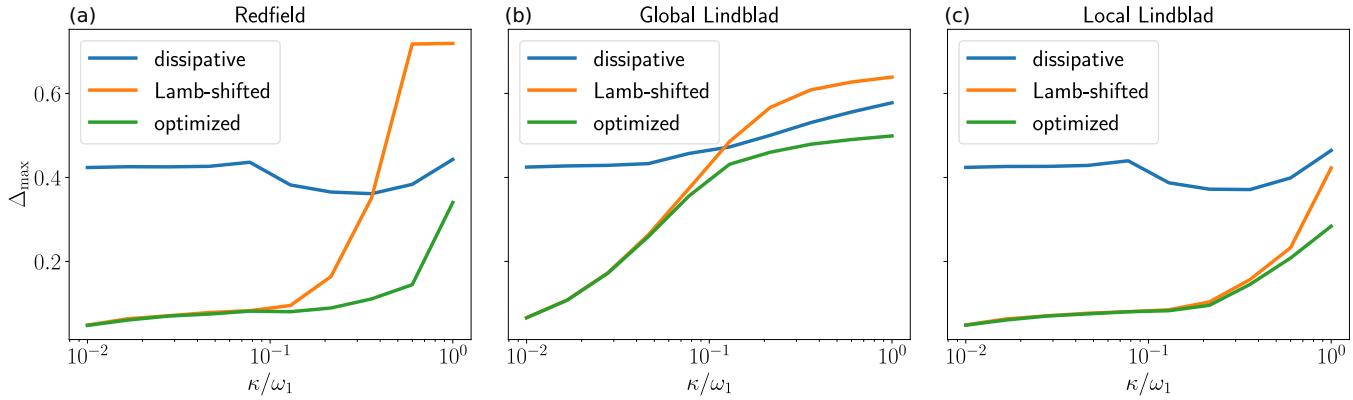

FIG. 9. Distance $\Delta_{\max}$ for nonoptimized purely dissipative (blue), Lamb-shifted (orange), and optimized (green) values of parameters at the low temperature $\hbar\omega_1\beta = 5$, $g = 0.1 \times \omega_1$. The number of samples in the SLED solutions is $N_{\text{traj}} = 5 \times 10^5$, and we have used the cutoff frequency $\omega_c/\omega_1 = 50$. For each value of κ, the distance is calculated for times $[0, 10^3\omega_1^{-1}]$.

least down to $T \approx 0.1 \times \hbar\omega_1/k_B$ ($\omega_q\hbar\beta \approx 10$), in the weak-coupling regime $\kappa \ll \omega_q$.

Note that whereas the nonoptimized results provide us information on the implications of the approximations carried out to arrive from the microscopic model to the approximate master equations, the optimized results may be considered as a test of the accuracy of the approaches as phenomenological models. In typical experiments, the latter case is important since the microscopic parameters may be inaccessible.

In the two-qubit case and at high bath temperatures, $T \gtrsim 10\omega_1/k_B$ ($\omega_1\hbar\beta \lesssim 0.1$), we find that the Redfield equation is valid ($\Delta_{\max} < 0.1$) in the whole parameter range studied ($\omega_1/100 < \kappa, g < \omega_1$ and $\kappa \lesssim 10g^2/\omega_1$). Interestingly, the global Lindblad approach is valid only for large enough qubit-qubit coupling $g \gtrsim 40\kappa$, whereas the local approach is valid only for $\kappa \lesssim 0.03 \times \omega_1$ and $g \lesssim 0.6 \times \omega_1$. Optimization of the model parameters extends validity of the local Lindblad method to intermediate qubit-qubit coupling $g \lesssim \omega_1$ and does not significantly change the validity bounds of the other approximate approaches. At intermediate and low T, we find $\Delta_{\max} > 0.1$ essentially in the whole parameter range considered.

With decreasing temperature, we observe a dramatically increasing deviation between the nonoptimized approximate and the exact dynamics. Optimization cures this discrepancy at weak coupling, but peculiarly, the point $\kappa \approx g$ seems problematic for weak-coupling approaches. We attribute this behavior to the failure of the BM equations to correctly capture the effect of the environment on the modes of the system in this point of critical damping for the qubit with an indirect coupling to the bath through the other qubit.

We conclude that as expected, the nonoptimized BM equations provide accurate dynamics only for weak coupling and high enough temperature for both single- and two-qubit systems. This, in turn, excludes them as sufficiently reliable tools for many important experimental scenarios. For superconducting qubits, we may have, for example, $\omega_q \approx 2\pi \times 10$ GHz and $T \approx 40$ mK, and hence $\omega_q\hbar\beta \approx 10$.

Using the optimization procedure, we demonstrated that the dynamics of the systems can be described by BM equations in broader ranges of parameters. However, the fitting of experimental data with BM equations beyond their regimes of validity may, in some cases, yield physically misleading parameter values for the system, the bath, and their coupling strengths.

In this paper, we have focused on comparing the most common BM methods examining their accuracy in different coupling and temperature regimes, which is most relevant for applications. Consequently, we did not focus on quantifying the nature and origin of non-Markovian effects, naturally present in the numerically exact dynamics. The microscopic origins of non-Markovian effects in open quantum systems constitute a highly nontrivial and interesting research question [17,80,81] that deserves further study.

ACKNOWLEDGMENTS

This research was financially supported by the European Research Council under Grant No. 681311 (QUESS), by the Academy of Finland through its Centre of Excellence in Quantum Technology (QTF) (Grants No. 312298 and No. 312300), by the Jane and Aatos Erkko Foundation, and by the Technology Industries of Finland Centennial Foundation. It was also supported by the German Science Foundation (Grants No. AN336/11-1 and No. AN336/12-1), the Centre for Integrated Quantum Science and Technology (IQ^{ST}), and the Zeiss Foundation under the grant TQuant. The authors wish to acknowledge CSC – IT Center for Science, Finland, for computational resources.

APPENDIX A: BORN-MARKOV MASTER EQUATIONS

The Liouville–von Neumann equation which describes the dynamics of the density operator of the total system has the form

$$\frac{d\hat{\rho}}{dt} = -\frac{i}{\hbar}[\hat{H}, \hat{\rho}]. \tag{A1}$$

We eliminate the bath and system Hamiltonian from the above equation by moving to the interaction picture:

$$\frac{d\hat{\tilde{\rho}}}{dt} = -\frac{i}{\hbar}[\hat{q}(t)\hat{\tilde{\xi}}(t), \hat{\tilde{\rho}}], \tag{A2}$$

where

$$\hat{\rho} = \exp\left[-\frac{it}{\hbar}\left(\hat{H}_{\mathrm{B}} + \hat{H}_{\mathrm{S}}\right)\right]\hat{\tilde{\rho}}\exp\left[\frac{it}{\hbar}\left(\hat{H}_{\mathrm{B}} + \hat{H}_{\mathrm{S}}\right)\right], \tag{A3}$$

$$\xi(t) = \sum_k g_k\left(\hat{b}_k^\dagger e^{i\omega_k t} + \hat{b}_k e^{-i\omega_k t}\right), \tag{A4}$$

and

$$\hat{q}(t) = \sum_{nm} q_{nm} e^{i(\varepsilon_n - \varepsilon_m)t/\hbar}|n\rangle\langle m|. \tag{A5}$$

Here, $|n\rangle$ is the nth eigenstate of the system Hamiltonian $\hat{H}_{\mathrm{S}}$, which corresponds to the eigenvalue ε_n. We follow the standard procedure and solve the density operator time evolution iteratively from (A2). Taking the iteration to second order, we reach the formal expression

$$\begin{aligned}\hat{\tilde{\rho}}(t) &= \hat{\tilde{\rho}}(0) - \frac{i}{\hbar}\int_0^t \left[\hat{q}(t')\hat{\tilde{\xi}}(t'), \hat{\tilde{\rho}}(t')\right]dt' \\ &= \hat{\tilde{\rho}}(0) - \frac{i}{\hbar}\int_0^t \left[\hat{q}(t')\hat{\tilde{\xi}}(t'), \hat{\tilde{\rho}}(0)\right]dt' \\ &\quad - \frac{1}{\hbar^2}\int_0^t\int_0^{t'} \left[\hat{q}(t')\hat{\tilde{\xi}}(t'), \left[\hat{q}(t'')\hat{\tilde{\xi}}(t''), \hat{\tilde{\rho}}(t'')\right]\right]dt'dt''\end{aligned} \tag{A6}$$

with the intent of substituting a (possibly approximate) analytic solution for the inner integration. For this purpose, one typically also assumes a factorized initial state

$$\hat{\tilde{\rho}}(0) = \hat{\tilde{\rho}}_{\mathrm{S}}(0)\otimes\hat{\rho}_{\mathrm{B}}, \tag{A7}$$

where $\hat{\tilde{\rho}}_{\mathrm{S}} = \mathrm{Tr}_{\mathrm{B}}\,\hat{\tilde{\rho}}$ and $\hat{\rho}_{\mathrm{B}} = \mathrm{Tr}_{\mathrm{S}}\,\hat{\tilde{\rho}}$ are the reduced density operators of the system and the bath, respectively. Moreover, if the coupling is weak, it is reasonable to assume that the correlations of the bath decay on a time scale τ_{B} much shorter than the relevant time scales in the interaction picture (relaxation and dephasing times). Assuming the differences $t - t'$ and $t - t''$ do not exceed this range, and assuming the rates are properly described as second-order effects, one can make the approximation

$$\hat{\tilde{\rho}}(t-\tau) \approx \hat{\tilde{\rho}}_{\mathrm{S}}(t-\tau)\otimes\hat{\rho}_{\mathrm{B}} \tag{A8}$$

on the terms $\hat{\tilde{\rho}}$ appearing on the right-hand side of Eq. (A6): Neglecting system-reservoir correlation effects at this point means neglecting effects of higher order in the interaction than second order. This constitutes the Born approximation on the coupled system-reservoir dynamics. Note that for factorizing initial states the Born-approximated dynamics cannot reveal even weak system-reservoir correlations unless the right-hand side of Eq. (A6) is evaluated in the full Liouville space.

Substituting (A8) into (A6) and taking into account that $\langle\hat{\tilde{\xi}}\rangle = \mathrm{Tr}_{\mathrm{B}}(\hat{\rho}_{\mathrm{B}}\hat{\tilde{\xi}}) = 0$, we obtain

$$\begin{aligned}\frac{d\hat{\tilde{\rho}}_{\mathrm{S}}}{dt} &= -\frac{1}{\hbar^2}\int_0^t \{[\hat{q}(t)\hat{q}(t')\hat{\tilde{\rho}}_{\mathrm{S}}(t') - \hat{q}(t')\hat{\tilde{\rho}}(t')\hat{q}(t)]\langle\hat{\tilde{\xi}}(t)\hat{\tilde{\xi}}(t')\rangle + [\hat{\tilde{\rho}}_{\mathrm{S}}(t')\hat{q}(t')\hat{q}(t) - \hat{q}(t)\tilde{\rho}_{\mathrm{S}}(t')\hat{q}(t')]\langle\hat{\tilde{\xi}}(t')\hat{\tilde{\xi}}(t)\rangle\}dt' \\ &= -\frac{1}{\hbar^2}\int_0^t \{[\hat{q}(t)\hat{q}(t-\tau)\hat{\tilde{\rho}}_{\mathrm{S}}(t-\tau) - \hat{q}(t-\tau)\hat{\tilde{\rho}}(t-\tau)\hat{q}(t)]\langle\hat{\tilde{\xi}}(t)\hat{\tilde{\xi}}(t-\tau)\rangle \\ &\quad + [\hat{\tilde{\rho}}_{\mathrm{S}}(t-\tau)\hat{q}(t-\tau)\hat{q}(t) - \hat{q}(t)\tilde{\rho}_{\mathrm{S}}(t-\tau)\hat{q}(t-\tau)]\langle\hat{\tilde{\xi}}(t-\tau)\hat{\tilde{\xi}}(t)\rangle\}d\tau,\end{aligned} \tag{A9}$$

where $\langle\hat{\tilde{\xi}}(t)\hat{\tilde{\xi}}(t-\tau)\rangle = \mathrm{Tr}_{\mathrm{B}}[\hat{\tilde{\xi}}(t)\hat{\tilde{\xi}}(t-\tau)\hat{\rho}_{\mathrm{B}}]$ is the bath correlation function. If the bath correlation function decays in a time scale τ_{B}, which is much shorter than any system time scale τ_{S}, one can approximate it with a function peaked at $\tau = 0$. In this limit, one typically makes the Markov approximation and assumes that $\hat{\tilde{\rho}}_{\mathrm{S}}(t-\tau) \sim \hat{\tilde{\rho}}_{\mathrm{S}}(t)$ in the region $\tau \lessapprox \tau_{\mathrm{B}}$ where the correlation function is appreciably different from zero. The time scale of the system in the interaction picture is again given by relaxation and dephasing, i.e., $\tau_{\mathrm{S}} \approx \kappa^{-1}$, where the rate κ characterizes the strength of the bath coupling. However, one cannot make a similar approximation for the operator $\hat{q}(t-\tau)$ as it obtains an oscillating phase of the form $e^{i(\varepsilon_n-\varepsilon_m)t/\hbar}$. For a bath in a thermal equilibrium with a smooth, broadband spectrum, the width of the correlation function is determined by the inverse temperature $\tau_{\mathrm{B}} \sim \hbar\beta$. Based on the above, the Markov approximation holds if $\hbar\kappa\beta \ll 1$. This is essentially the same condition used to justify the Born approximation. If the times t under consideration obey $t \gg \hbar\beta$, one can extend the limits of the integration in Eq. (A9) to infinity, neglecting an initial slip which is typically insignificant. Thus one obtains

$$\begin{aligned}\frac{d\hat{\tilde{\rho}}_{\mathrm{S}}}{dt} &= -\frac{1}{\hbar^2}\int_0^{+\infty} \{[\hat{q}(t)\hat{q}(t-\tau)\hat{\tilde{\rho}}_{\mathrm{S}}(t) - \hat{q}(t-\tau)\hat{\tilde{\rho}}_{\mathrm{S}}(t)\hat{q}(t)]\langle\hat{\tilde{\xi}}(t)\hat{\tilde{\xi}}(t-\tau)\rangle \\ &\quad + [\hat{\tilde{\rho}}_{\mathrm{S}}(t)\hat{q}(t-\tau)\hat{q}(t) - \hat{q}(t)\tilde{\rho}_{\mathrm{S}}(t)\hat{q}(t-\tau)]\langle\hat{\tilde{\xi}}(t-\tau)\hat{\tilde{\xi}}(t)\rangle\}d\tau.\end{aligned} \tag{A10}$$

In the literature, this is referred to as the Born-Markov master equation of the reduced system density operator. In the Schrödinger picture, each of the individual terms describes a particular form of simultaneous propagation of system and reservoir between two interactions, graphically represented in the Feynman diagrams of Fig. 10. We remark that the justification of the Born approximation from the inequality $\hbar\kappa\beta \ll 1$ alone is not fully rigorous. For the typical case of reservoirs with a smooth and monotonically rising density of states, higher-order corrections seem to be irrelevant at temperatures low enough compared with energy splittings of the system [82].

Performing integration over τ in Eq. (A10) and neglecting the correction to the coherent part of the Hamiltonian (the

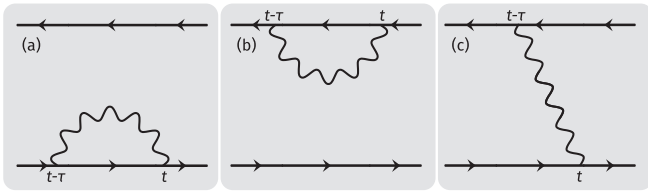

FIG. 10. Schematic Feynman diagrams of processes implied in Markovian master equations. Solid lines represent system propagation; wiggly lines represent reservoir (de-)excitations. Diagrams (a) and (b) are self-energy-like corrections to the left or right application of the system Hamiltonian; (c) represents real emission or absorption. The partial trace implied by the reduced density matrix prevents the appearance of open in- or outgoing reservoir lines.

Lamb shift), one obtains the Redfield master equation. By making a transformation back to the Schrödinger picture, the Redfield equation can be written in the eigenbasis of the Hamiltonian $\hat{H}_S$ as

$$\dot{\rho}_{jk} = i\omega_{jk}\rho_{jk} - \sum_{lm} R_{jklm}\rho_{lm}, \tag{A11}$$

where

$$R_{jklm} = \frac{1}{2\hbar^2}\Big\{\delta_{km}\sum_n S(\omega_{nl})q_{jn}q_{nl} + \delta_{jl}\sum_n S(-\omega_{mn})q_{mn}q_{nk} - [S(\omega_{jl}) + S(-\omega_{mk})]q_{jl}q_{mk}\Big\} \tag{A12}$$

and $q_{nm} = \langle n|\hat{q}|m\rangle$, $\omega_{nm} = \omega_m - \omega_n$, $\hat{H}_S|n\rangle = \hbar\omega_n|n\rangle$, and $S(\omega)$ is the Fourier image of the bath correlation function:

$$S(\omega) = \int_{-\infty}^{+\infty}\langle\hat{\xi}(t)\hat{\xi}(t-\tau)\rangle e^{i\omega\tau}d\tau = \frac{2\hbar J(\omega)}{1-e^{-\hbar\beta\omega}}. \tag{A13}$$

The last equation holds for the bath in the thermal equilibrium.

The Lindblad equation is obtained from the Redfield equation written in the interaction picture using the secular approximation. For a system with a nondegenerate spectrum the Lindblad equation, restricted to diagonal states in the eigenbasis of the Hamiltonian $\hat{H}_S$, reads

$$\dot{\rho}_{nn} = \sum_m [\Gamma_{m\to n}\rho_{mm} - \Gamma_{n\to m}\rho_{nn}], \tag{A14}$$

where we have denoted reservoir-induced transition rates between the eigenstates by

$$\Gamma_{m\to n} = \frac{|q_{nm}|^2}{\hbar^2}S(-\omega_{mn}). \tag{A15}$$

Thus the diagonal density matrix elements are decoupled from the off-diagonal ones. The temporal evolution of the off-diagonal terms can also be calculated, and we find that they approach the steady state as

$$\dot{\rho}_{nm} = i\omega_{nm}\rho_{nm} - \big(\gamma_{nm} + \gamma^{\phi}_{nm}\big)\rho_{nm}, \tag{A16}$$

where the losses in the phase coherence are caused by relaxation,

$$\gamma_{nm} = \frac{1}{2}\sum_{k\neq n,m}[\Gamma_{n\to k} + \Gamma_{m\to k}], \tag{A17}$$

and pure dephasing,

$$\gamma^{\phi}_{nm} = \frac{1}{2\hbar^2}S(0)[q_{nn} - q_{mm}]^2, \tag{A18}$$

between the states $|n\rangle$ and $|m\rangle$.

Alternatively, one may represent the time dependence of the interaction picture operators $\hat{q}(t)$ and $\hat{q}(t-\tau)$ in Eq. (A10) through eigenoperators [12] of the superoperator $[H_S, \cdot]$. For a harmonic oscillator, for example, these are the raising and lowering operators. Thus the secular approximation leads to neglecting the terms in Eq. (A10) that oscillate at the system frequencies and keeping those terms which are constants with respect to t. This procedure is meaningful only if the damping is weak enough to permit a significant number of oscillation cycles between emission events, i.e., if the relaxation and dephasing rates are lower than all transition frequencies. This approach leads directly to the commonly used general form of a Lindblad master equation,

$$\frac{d\hat{\rho}_S}{dt} = -\frac{i}{\hbar}[H, \hat{\rho}_S] + \sum_\alpha \gamma_\alpha\left(L_\alpha\hat{\rho}_S L_\alpha^\dagger - \frac{1}{2}\{L_\alpha^\dagger L_\alpha, \hat{\rho}_S\}\right). \tag{A19}$$

In the case of weakly interacting qubits, the introduction of yet another small parameter g complicates both the determination of eigenoperators and the application of the secular approximation. If g is small, the assumptions used in the construction of the Lindblad master equation are easily violated. However, in the case where g is even smaller than the relaxation and dephasing rates, one may altogether neglect it in the construction of the Lindbladian, which leads to the *local* Lindblad approach.

Lamb shift

In deriving the above equations (A11), (A14), and (A16), we neglected a coherent contribution to the Hamiltonian, the Lamb shift, which is important in the low-temperature limit. This coherent correction can be found by carrying out an integration over τ in Eq. (A10) yielding

$$\hat{H}_{\rm LS} = -\frac{1}{2\pi\hbar^2}\sum_{klm}\mathrm{PV}\int\frac{q_{kl}q_{lm}|k\rangle\langle m|}{\omega-\omega_{lm}}S(\omega)d\omega, \tag{A20}$$

where PV stands for the principal value of the integral. We note that this correction, in general, does not commute with the bare Hamiltonian of the system $\hat{H}_S$. If we apply the rotating-wave approximation in order to obtain the Lindblad equation, only diagonal terms of the correction survive since the off-diagonal terms oscillate in the interaction picture. Consequently, we obtain

$$\hat{H}^{\rm rw}_{\rm LS} = -\frac{1}{2\pi\hbar^2}\sum_{lm}\mathrm{PV}\int\frac{|q_{ml}|^2|m\rangle\langle m|}{\omega-\omega_{lm}}S(\omega)d\omega. \tag{A21}$$

APPENDIX B: STOCHASTIC LIOUVILLE EQUATIONS

The time evolution is solved from the stochastic Liouville-von Neumann (SLN) equation, which can be written into the

form

$$i\hbar\frac{d\hat{\rho}_S}{dt} = [\hat{H}_S, \hat{\rho}_S] - \zeta[\hat{q}, \hat{\rho}_S] - \frac{\hbar}{2}\nu\{\hat{q}, \hat{\rho}_S\}, \tag{B1}$$

where ζ and ν are complex noise terms that arise from exact treatment of the coupling in the path-integral formalism. Together with the anticommutator, these terms result in nonunitary time evolution for individual samples, i.e., realizations of the noise terms. However, by making a stochastic average, the non-Hermitian parts of the density operator vanish. Also the trace of the density operator is unity on average. The noise terms obey the correlation functions

$$\langle\zeta(t)\zeta(t')\rangle = \mathrm{Re}\, L(t-t'), \tag{B2}$$

$$\begin{aligned}\langle\zeta(t)\nu(t')\rangle &= \frac{2i}{\hbar}\Theta(t-t')\,\mathrm{Im}\, L(t-t') + i\mu\delta(t-t') \\ &= -i\chi_R(t-t') + i\mu\delta(t-t'),\end{aligned} \tag{B3}$$

$$\langle\nu(t)\nu(t')\rangle = 0. \tag{B4}$$

Above, the bath correlation function

$$L(t-t') = \frac{\hbar}{\pi}\int_0^{+\infty} d\omega J(\omega)\left\{\coth\left(\frac{\hbar\beta\omega}{2}\right)\cos[\omega(t-t')] - i\sin[\omega(t-t')]\right\}, \tag{B5}$$

and we have defined the classical response function

$$\chi_R(t) = -\frac{2}{\hbar}\Theta(t)\,\mathrm{Im}\, L(t) \tag{B6}$$

and

$$\mu = \int_{-\infty}^{+\infty} dt\,\chi_R(t). \tag{B7}$$

In the case of the ohmic spectral density with a Drude cutoff, defined in (3) where the cutoff frequency ω_c is much larger than any other frequency in the system, one can write the SLN equation into the form of the stochastic Liouville equation with dissipation (SLED),

$$\begin{aligned}i\hbar\frac{d\hat{\rho}}{dt} = [\hat{H}_S, \hat{\rho}] - \frac{i\eta}{\hbar\beta}[\hat{q}, [\hat{q}, \hat{\rho}]] \\ + \frac{i\eta}{2\hbar}[\hat{q}, \{[\hat{H}_S, \hat{q}], \hat{\rho}\}] - \zeta[\hat{q}, \hat{\rho}_S],\end{aligned} \tag{B8}$$

where $\zeta(t)$ is a stochastic Gaussian process with the following correlation function:

$$\begin{aligned}&\langle\zeta(t)\zeta(t')\rangle \\ &= \frac{\hbar}{\pi}\int_0^{+\infty} d\omega J(\omega)\left[\coth\left(\frac{\hbar\beta\omega}{2}\right) - \frac{2}{\hbar\beta\omega}\right]\cos[\omega(t-t')].\end{aligned} \tag{B9}$$

Notice that the assumption of the large cutoff frequency is used only in the noise process ν; the cutoff frequency is still present in the autocorrelation function of ζ. As a consequence of this approximation, the two complex noise terms in the SLN equation have been reduced into a deterministic part and a single real-valued noise term.

[1] D. P. DiVincenzo, Fortschr. Phys. **48**, 771 (2000).

[2] M. A. Nielsen and I. L. Chuang, *Quantum Computation and Quantum Information* (Cambridge University Press, New York, 2000).

[3] F. Arute, K. Arya, R. Babbush, D. Bacon, J. C. Bardin, R. Barends, R. Biswas, S. Boixo, F. G. S. L. Brandao, D. A. Buell, B. Burkett, Y. Chen, Z. Chen, B. Chiaro, R. Collins, W. Courtney, A. Dunsworth, E. Farhi, B. Foxen, A. Fowler *et al.*, Nature (London) **574**, 505 (2019).

[4] M. Kjaergaard, M. E. Schwartz, J. Braumüller, P. Krantz, J. I.-J. Wang, S. Gustavsson, and W. D. Oliver, Annu. Rev. Condens. Matter Phys. **11**, 369 (2020).

[5] A. Blais, A. L. Grimsmo, S. M. Girvin, and A. Wallraff, Rev. Mod. Phys. **93**, 025005 (2021).

[6] R. Kosloff and A. Levy, Annu. Rev. Phys. Chem. **65**, 365 (2014).

[7] D. Newman, F. Mintert, and A. Nazir, Phys. Rev. E **95**, 032139 (2017).

[8] J. Klatzow, J. N. Becker, P. M. Ledingham, C. Weinzetl, K. T. Kaczmarek, D. J. Saunders, J. Nunn, I. A. Walmsley, R. Uzdin, and E. Poem, Phys. Rev. Lett. **122**, 110601 (2019).

[9] D. von Lindenfels, O. Gräb, C. T. Schmiegelow, V. Kaushal, J. Schulz, M. T. Mitchison, J. Goold, F. Schmidt-Kaler, and U. G. Poschinger, Phys. Rev. Lett. **123**, 080602 (2019).

[10] U. Weiss, *Quantum Dissipative Systems*, Series in Modern Condensed Matter Physics (World Scientific, Singapore, 2012), Vol. 13.

[11] A. J. Leggett, S. Chakravarty, A. T. Dorsey, M. P. A. Fisher, A. Garg, and W. Zwerger, Rev. Mod. Phys. **59**, 1 (1987); **67**, 725(E) (1995).

[12] H. P. Breuer and F. Petruccione, *The Theory of Open Quantum Systems* (Oxford University Press, Oxford, 2002).

[13] Á. Rivas and S. Huelga, *Open Quantum Systems: An Introduction*, SpringerBriefs in Physics (Springer, Berlin, 2011).

[14] J. Ankerhold, P. Pechukas, and H. Grabert, Phys. Rev. Lett. **87**, 086802 (2001).

[15] D. Braun, F. Haake, and W. T. Strunz, Phys. Rev. Lett. **86**, 2913 (2001).

[16] J. Salmilehto, P. Solinas, and M. Möttönen, Phys. Rev. E **89**, 052128 (2014).

[17] I. de Vega and D. Alonso, Rev. Mod. Phys. **89**, 015001 (2017).

[18] D. Xu and J. Cao, Front. Phys. **11**, 110308 (2016).

[19] A. Ishizaki, T. R. Calhoun, G. S. Schlau-Cohen, and G. R. Fleming, Phys. Chem. Chem. Phys. **12**, 7319 (2010).

[20] C. Gardiner and P. Zoller, *Quantum Noise: A Handbook of Markovian and Non-Markovian Quantum Stochastic Methods with Applications to Quantum Optics* (Springer, New York, 2004).

[21] A. Redfield, *Advances in Magnetic and Optical Resonance* (Elsevier, New York, 1965), Vol. 1, pp. 1–32..

[22] G. Lindblad, Commun. Math. Phys. **48**, 119 (1976).

[23] V. Gorini, A. Kossakowski, and E. C. G. Sudarshan, J. Math. Phys. (Melville, NY) **17**, 821 (1976).

[24] J. Tuorila, J. Stockburger, T. Ala-Nissila, J. Ankerhold, and M. Möttönen, Phys. Rev. Research **1**, 013004 (2019).

[25] P. Jones, J. Huhtamäki, J. Salmilehto, K. Tan, and M. Möttönen, Sci. Rep. **3**, 1987 (2013).

[26] J. Tuorila, M. Partanen, T. Ala-Nissila, and M. Möttönen, npj Quantum Inf. **3**, 27 (2017).

[27] S. O. Valenzuela, W. D. Oliver, D. M. Berns, K. K. Berggren, L. S. Levitov, and T. P. Orlando, Science **314**, 1589 (2006).

[28] M. Grajcar, S. Van der Ploeg, A. Izmalkov, E. Il'ichev, H.-G. Meyer, A. Fedorov, A. Shnirman, and G. Schön, Nat. Phys. **4**, 612 (2008).

[29] K. Geerlings, Z. Leghtas, I. M. Pop, S. Shankar, L. Frunzio, R. J. Schoelkopf, M. Mirrahimi, and M. H. Devoret, Phys. Rev. Lett. **110**, 120501 (2013).

[30] X. Y. Jin, A. Kamal, A. P. Sears, T. Gudmundsen, D. Hover, J. Miloshi, R. Slattery, F. Yan, J. Yoder, T. P. Orlando, S. Gustavsson, and W. D. Oliver, Phys. Rev. Lett. **114**, 240501 (2015).

[31] J. Ankerhold and J. P. Pekola, Phys. Rev. B **90**, 075421 (2014).

[32] T. Motz, M. Wiedmann, J. T. Stockburger, and J. Ankerhold, New J. Phys. **20**, 113020 (2018).

[33] M. Wiedmann, J. T. Stockburger, and J. Ankerhold, New J. Phys. **22**, 033007 (2020).

[34] J. Senior, A. Gubaydullin, B. Karimi, J. T. Peltonen, J. Ankerhold, and J. P. Pekola, Commun. Phys. **3**, 40 (2020).

[35] A. Levy and R. Kosloff, Europhys. Lett. **107**, 20004 (2014).

[36] J. O. González, L. A. Correa, G. Nocerino, J. P. Palao, D. Alonso, and G. Adesso, Open Syst. Inf. Dyn. **24**, 1740010 (2017).

[37] G. D. Chiara, G. Landi, A. Hewgill, B. Reid, A. Ferraro, A. J. Roncaglia, and M. Antezza, New J. Phys. **20**, 113024 (2018).

[38] K. Y. Tan, M. Partanen, R. E. Lake, J. Govenius, S. Masuda, and M. Möttönen, Nat. Commun. **8**, 15189 (2017).

[39] M. Silveri, H. Grabert, S. Masuda, K. Y. Tan, and M. Möttönen, Phys. Rev. B **96**, 094524 (2017).

[40] V. Sevriuk, K. Y. Tan, E. Hyyppä, M. Silveri, M. Partanen, M. Jenei, S. Masuda, J. Goetz, V. Vesterinen, L. Grönberg, and M. Möttönen, Appl. Phys. Lett. **115**, 082601 (2019).

[41] M. Silveri, S. Masuda, V. Sevriuk, K. Y. Tan, M. Jenei, E. Hyyppä, F. Hassler, M. Partanen, J. Goetz, R. E. Lake, L. Grönberg, and M. Möttönen, Nat. Phys. **15**, 533 (2019).

[42] P. Magnard, P. Kurpiers, B. Royer, T. Walter, J.-C. Besse, S. Gasparinetti, M. Pechal, J. Heinsoo, S. Storz, A. Blais, and A. Wallraff, Phys. Rev. Lett. **121**, 060502 (2018).

[43] J. P. Pekola, Nat. Phys. **11**, 118 (2015).

[44] Y. Makhlin, G. Schön, and A. Shnirman, Rev. Mod. Phys. **73**, 357 (2001).

[45] F. Verstraete, M. M. Wolf, and J. I. Cirac, Nat. Phys. **5**, 633 (2009).

[46] M. J. Kastoryano, F. Reiter, and A. S. Sørensen, Phys. Rev. Lett. **106**, 090502 (2011).

[47] D. D. Bhaktavatsala Rao and K. Mølmer, Phys. Rev. A **90**, 062319 (2014).

[48] A. A. Houck, H. E. Türeci, and J. Koch, Nat. Phys. **8**, 292 (2012).

[49] M. Fitzpatrick, N. M. Sundaresan, A. C. Y. Li, J. Koch, and A. A. Houck, Phys. Rev. X **7**, 011016 (2017).

[50] R. Ma, B. Saxberg, C. Owens, N. Leung, Y. Lu, J. Simon, and D. I. Schuster, Nature (London) **566**, 51 (2019).

[51] R. P. Feynman and F. L. Vernon, Ann. Phys. (Amsterdam) **24**, 118 (1963).

[52] D. Kast and J. Ankerhold, Phys. Rev. Lett. **110**, 010402 (2013).

[53] L. Diosi and W. T. Strunz, Phys. Lett. A **235**, 569 (1997).

[54] J. T. Stockburger and H. Grabert, Phys. Rev. Lett. **88**, 170407 (2002).

[55] J. T. Stockburger, Chem. Phys. **296**, 159 (2004).

[56] R. Schmidt, A. Negretti, J. Ankerhold, T. Calarco, and J. T. Stockburger, Phys. Rev. Lett. **107**, 130404 (2011).

[57] R. Schmidt, J. T. Stockburger, and J. Ankerhold, Phys. Rev. A **88**, 052321 (2013).

[58] J. T. Stockburger and C. H. Mak, Phys. Rev. Lett. **80**, 2657 (1998).

[59] J. T. Stockburger and C. H. Mak, J. Chem. Phys. **110**, 4983 (1999).

[60] E. B. Davies, Commun. Math. Phys. **39**, 91 (1974).

[61] S. Alipour, A. T. Rezakhani, A. P. Babu, K. Mølmer, M. Möttönen, and T. Ala-Nissila, Phys. Rev. X **10**, 041024 (2020).

[62] A. Verso and J. Ankerhold, Phys. Rev. A **81**, 022110 (2010).

[63] V. Gramich, S. Gasparinetti, P. Solinas, and J. Ankerhold, Phys. Rev. Lett. **113**, 027001 (2014).

[64] P. P. Hofer, M. Perarnau-Llobet, L. D. M. Miranda, G. Haack, R. Silva, J. B. Brask, and N. Brunner, New J. Phys. **19**, 123037 (2017).

[65] G. Deçordi and A. Vidiella-Barranco, Opt. Commun. **387**, 366 (2017).

[66] M. Cattaneo, G. L. Giorgi, S. Maniscalco, and R. Zambrini, New J. Phys. **21**, 113045 (2019).

[67] M. Möttönen, J. J. Vartiainen, and J. P. Pekola, Phys. Rev. Lett. **100**, 177201 (2008).

[68] J. P. Pekola, V. Brosco, M. Möttönen, P. Solinas, and A. Shnirman, Phys. Rev. Lett. **105**, 030401 (2010).

[69] J. Salmilehto and M. Möttönen, Phys. Rev. B **84**, 174507 (2011).

[70] J. Salmilehto, P. Solinas, and M. Möttönen, Phys. Rev. A **85**, 032110 (2012).

[71] H. Grabert, P. Schramm, and G.-L. Ingold, Phys. Rep. **168**, 115 (1988).

[72] A. Ishizaki and Y. Tanimura, J. Phys. Soc. Jpn. **74**, 3131 (2005).

[73] Y. Tanimura, J. Chem. Phys. **153**, 020901 (2020).

[74] N. Makri, J. Math. Phys. (Melville, NY) **36**, 2430 (1995).

[75] N. Makri, J. Phys. Chem. A **102**, 4414 (1998).

[76] J. Prior, A. W. Chin, S. F. Huelga, and M. B. Plenio, Phys. Rev. Lett. **105**, 050404 (2010).

[77] A. W. Chin, Á. Rivas, S. F. Huelga, and M. B. Plenio, J. Math. Phys. (Melville, NY) **51**, 092109 (2010).

[78] P. Virtanen, R. Gommers, T. E. Oliphant, M. Haberland, T. Reddy, D. Cournapeau, E. Burovski, P. Peterson, W. Weckesser, J. Bright, S. J. van der Walt, M. Brett, J. Wilson, K. J. Millman, N. Mayorov, A. R. J. Nelson, E. Jones, R. Kern, E. Larson, C. Carey *et al.*, Nat. Methods **17**, 261 (2020).

[79] See Supplemental Material at http://link.aps.org/supplemental/10.1103/PhysRevB.103.214308 for values of optimization parameters.

[80] A. P. Babu, S. Alipour, A. T. Rezakhani, and T. Ala-Nissila, arXiv:2104.04248.

[81] H.-P. Breuer, E.-M. Laine, J. Piilo, and B. Vacchini, Rev. Mod. Phys. **88**, 021002 (2016).

[82] F. Napoli, M. Sassetti, and U. Weiss, Phys. B (Amsterdam) **202**, 80 (1994).